Matter

CellPress

Article

Electronic Blood Vessel

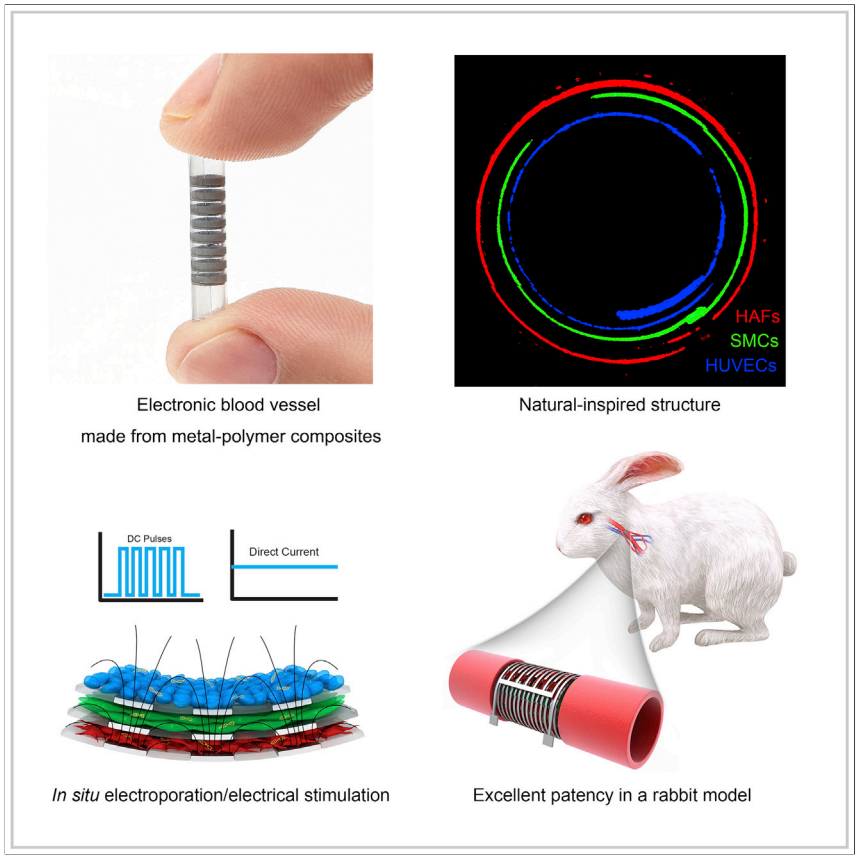

Integrating bioelectronics and living tissues could enable powerful functionalities and capabilities to overcome biomedical problems. Here we introduce an electronic blood vessel that can integrate the conducting liquid metal-polymer circuitry with three layers of blood-vessel cells, to mimic and go beyond the natural blood vessel. With excellent biocompatibility and mechanical properties, it enables electrical stimulation and electroporation and exhibits great patency in a rabbit model.

Shiyu Cheng, Chen Hang, Li Ding, ..., Wenfu Zheng, Yan Zhang, Xingyu Jiang

jiang@sustech.edu.cn (X.J.)
waikezhangyan@126.com (Y.Z.)

HIGHLIGHTS

Electronic blood vessel consists of biodegradable polymer and metal-polymer conductor

Electrical stimulation promotes HUVEC proliferation and migration *in situ*

Electroporation enables controlled gene delivery in different blood-vessel cell layers

Excellent compatibility in the vascular system and great patency in a rabbit model

4 **Demonstrate**
Proof-of-concept of performance with intended application/response

Cheng et al., Matter *3*, 1–21
November 4, 2020
https://doi.org/10.1016/j.matt.2020.08.029

Please cite this article in press as: Cheng et al., Electronic Blood Vessel, Matter (2020), https://doi.org/10.1016/j.matt.2020.08.029

Matter

CellPress

Article

Electronic Blood Vessel

Shiyu Cheng,[1,2,4,5] Chen Hang,[1,2,5] Li Ding,[1,2,3,5] Liujun Jia,[3] Lixue Tang,[2] Lei Mou,[1,2] Jie Qi,[1,2] Ruihua Dong,[1,2] Wenfu Zheng,[2] Yan Zhang,[3,*] and Xingyu Jiang[1,2,6,*]

SUMMARY

Advances in bioelectronics have great potential to address unsolved biomedical problems in the cardiovascular system. By using poly (L-lactide-co-ϵ-caprolactone), which encapsulates liquid metal to make flexible and biodegradable electrical circuitry, we develop an electronic blood vessel that can integrate flexible electronics with three layers of blood-vessel cells, to mimic and go beyond the natural blood vessel. It can improve the endothelialization process through electrical stimulation and can enable controlled gene delivery into specific parts of the blood vessel via electroporation. The electronic blood vessel has excellent biocompatibility in the vascular system and shows great patency 3 months post-implantation in a rabbit model. The electronic blood vessel would be an ideal platform to enable diagnostics and treatments in the cardiovascular system and can greatly empower personalized medicine by creating a direct link of the vascular tissue-machine interface.

INTRODUCTION

Cardiovascular diseases remain the number one cause of mortality worldwide.[1] In the treatment of cardiovascular diseases via coronary artery bypass grafting surgery, no existing small-diameter (<6 mm) tissue engineered blood vessel (TEBV) has met clinical demands.[2] To fabricate the TEBV, a range of approaches, such as decellularized matrix,[3–7] self-assembly cell sheets,[8–11] and bioactive and biomimetic materials,[12–14] have been developed and clinically investigated in recent years. However, most of these methods serve only as scaffolds to provide mechanical support and rely mainly on the remodeling process of the host tissue and present significant limitations in helping the regeneration of new blood vessels. Thus far, none of them have achieved satisfactory clinical results. Specifically, a complex interplay between the blood flow and the TEBV can often cause inflammatory responses, resulting in thrombosis, neointimal hyperplasia, or smooth muscle cell accumulation near the scaffold,[2,15] in different pathological stages. To address these issues, next-generation TEBVs should not only function as scaffolds to provide the mechanical support and facilitate host cell recruitments, but also have the capability to actively respond to and couple with the native remodeling process in order to provide adaptive treatments after implantation.

Combining living tissues with flexible electronics[16,17] could endow the conventional TEBV with more functionalities and capabilities to overcome existing biomedical problems, such as precision diagnostics, by sensing the blood flow and temperature *in situ*, and treatments by therapeutic drug or gene delivery.[18,19] In previous work, we have developed many approaches to fabricate structures that mimic natural blood vessels with multiple types of blood-vessel cells in different layers, including the stress-induced self-rolling membrane[13,20–22] and layer-by-layer techniques.[23] Recently, we have developed a printable metal-polymer conductor (MPC), which exhibited excellent

Progress and Potential

Existing small-diameter (<6 mm) tissue engineered blood vessels (TEBVs) rely mainly on the host remodeling progress and cannot provide further diagnostics or therapeutics in response to various pathological issues after implantation. Here we report an electronic blood vessel, with excellent biocompatibility, flexibility, mechanical strength, and degradability, that could enable *in situ* electrical stimulation (to facilitate the endothelialization process) and electroporation (to deliver genes in specific layers of blood-vessel cells) and exhibit excellent patency in a rabbit model. It endows electrical function on conventional biodegradable TEBVs and provides us with a new platform for tackling problems threatening the small-diameter blood vessel. When combined with emerging technologies such as artificial intelligence, it can greatly boost future personalized medicine by bridging the vascular tissue-machine interface and empowering health data collection/storage and early intervention.

compatibility and high stretchability.[24,25] Here, we develop an electronic blood vessel that integrates flexible electrodes into the biodegradable scaffold by combining liquid metal with poly(L-lactide-co-ϵ-caprolactone) (PLC) into an MPC. As a proof of concept, we used the electronic blood vessel to carry out *in vitro* electrical stimulation and electroporation. By electrical stimulation, the electronic blood vessel can effectively promote cell proliferation and migration in a wound healing model. It can also deliver a green fluorescent protein (GFP) DNA plasmid *in situ* into three kinds of blood-vessel cells via electroporation. We evaluated the efficacy and biosafety of the electronic blood vessel in the vascular system through a 3-month *in vivo* study by using a rabbit carotid artery replacement model and confirmed its patency through ultrasound imaging and arteriography. Our results pave the way to integrating flexible, degradable bioelectronics into the vascular system, which can serve as a platform to carry out further treatments, such as gene therapies, electrical stimulation, and electronically controlled drug release.

RESULTS

Fabrication of the Electronic Blood Vessel

We fabricated the electronic blood vessel (Figure 1A) by rolling up a PLC-based MPC (MPC-PLC) membrane (Figure 1B) with the assistance of a polytetrafluoroethylene (PTFE) mandrel. The MPC circuit was well distributed in the three-dimensional (3D) multilayered tubular structure. The inner diameter of the electronic blood vessel was around 2 mm (Figure 1A) and the minimum diameter could be around 0.5 mm (Figure S1A). The MPC-PLC membrane is flexible and degradable, and the MPC circuit is conductive (Figures 1B–1D). The conductivity of the MPC circuit is about 8×10^3 S cm^{-1} and the $\Delta R/R$ of the circuit remained constant after around 1,000 cycles of bending and rubbing (Figure 1C). The PLC is projected to be entirely degraded by around 1–2 years by the manufacturer. The MPC-PLC membrane underwent a mass loss of around 10% during an 8-week incubation in PBS (37°C) (Figure 1D). We observed a relatively quick degradation in the first week (Figure S2). To fabricate the MPC-PLC membrane, we screen-printed conductive ink on a polyethylene terephthalate (PET) membrane (Figure 1E). The electrode design was optimized for electroporation and electrical stimulation. By preparing different electrode designs, we could either target individual blood-vessel layers (tunica intima/media/adventitia) with the electrodes distributed in specific areas or target all three layers with the full electrode (Figures S1B and S1C). We prepared the liquid metal conductive ink by sonicating a mixture of gallium-indium alloy (EGAIn, ≥99.99%, Sigma, USA) and a volatile solvent (1-decanol, Macklin, Shanghai) (Figures 1F and 1H). The liquid metal particles (LMPs) exhibit a core-shell structure, where the core is the Ga-In alloy and the shell is the Ga-In oxide (Figure 1G). The diameter of the LMPs is around 2 μm (Figure 1J). We embedded the LMP-based circuit in the PLC solution (5 wt% in CH_2Cl_2) and peeled the MPC-PLC membrane off the PET substrate after evaporation of the solvent in a chemical hood (Figure 1E). The thickness of the MPC-PLC membrane is about 50 μm and it is tunable by changing the volume of the PLC solution. The LMPs could be broken during the process of peeling and release the Ga-In alloy to make the circuit conductive.[25] We confirmed the structure of the conductive circuit via corrosion of the Ga-In alloy by adding excessive hydrochloric acid (Beijing Chemical Works, China). The LMPs were evenly distributed in the cellular PLC host (Figures 1K and 1L). The liquid metal could form a coherent conductive pathway in the polymeric host.

In Vitro Characterization of the Electronic Blood Vessel

To evaluate the biocompatibility of the electronic blood vessel, we used microfluidic technology to realize an accurate 3D pattern of three kinds of blood-vessel cells in a

[1]Department of Biomedical Engineering and Shenzhen Bay Laboratory, Southern University of Science and Technology, Shenzhen, Guangdong 518055, China

[2]National Center for NanoScience and Technology, University of Chinese Academy of Sciences, Beijing 100190, China

[3]State Key Laboratory of Cardiovascular Disease, Fuwai Hospital, National Center for Cardiovascular Diseases, Chinese Academy of Medical Sciences and Peking Union Medical College, Beijing 100037, China

[4]Present address: Institute of Bioengineering, School of Engineering, Ecole Polytechnique Fédérale de Lausanne, Lausanne 1015, Switzerland

[5]These authors contributed equally

[6]Lead Contact

*Correspondence: jiang@sustech.edu.cn (X.J.), waikezhangyan@126.com (Y.Z.)

https://doi.org/10.1016/j.matt.2020.08.029

Please cite this article in press as: Cheng et al., Electronic Blood Vessel, Matter (2020), https://doi.org/10.1016/j.matt.2020.08.029

CellPress

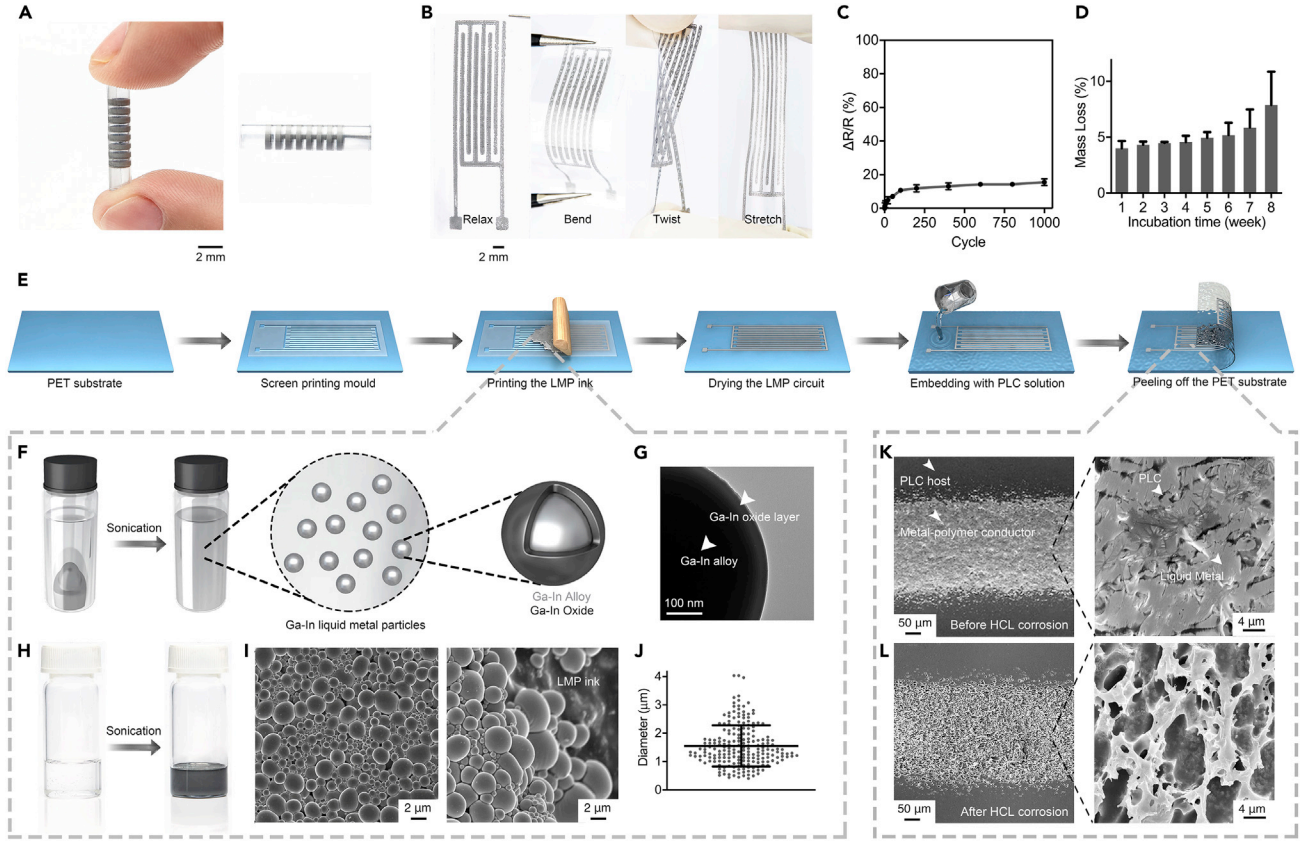

Figure 1. Fabrication and Characterization of the Electronic Blood Vessel

(A) Snapshots of the electronic blood vessel. Scale bar, 2 mm.

(B) Snapshots of the MPC-PLC membrane. Scale bar, 2 mm.

(C) ΔR/R changes with a bend of 180° for 1,000 cycles (n = 3).

(D) Mass loss of the MPC-PLC membrane during 8-week incubation (n = 3 for each time point).

(E) Schematic of fabrication of the MPC-PLC membrane.

(F) Schematic of fabrication of LMPs.

(G) Transmission electron microscopy image of the Ga-In particle. Scale bar, 100 nm.

(H) Photographs of mixture of the Ga-In alloy and the solvent, and the LMP ink after sonication.

(I) Representative scanning electron microscopy (SEM) images of LMPs. Scale bar, 2 μm.

(J) Diameter distribution of LMPs (n = 200).

(K) SEM images of the MPC-PLC circuit. White arrowheads indicate the PLC host and MPC-PLC membrane. Scale bar, 50 μm. Right is the zoom-in view. White arrowheads indicate the PLC and LMP ink. LMPs were embedded by the PLC as the host polymer. Scale bar, 4 μm.

(L) SEM images of the MPC-PLC circuit after corrosion by excessive hydrochloric acid. Scale bar, 50 μm. Right is the zoom-in view. LMPs were fully removed by corrosion. The porous structure consisted of only the PLC. Scale bar, 4 μm.

natural blood-vessel mimicking fashion. By employing a multichannel microfluidic chip, we delivered human umbilical vein endothelial cells (HUVECs, blue), human aortic smooth muscle cells (SMCs, green), and human aortic fibroblasts (HAFs, red) sequentially on the MPC-PLC membrane (Figures 2A–2E). We designed the width of each channel to match the circumference of each layer of the tube based on the thickness of the MPC-PLC membrane and the diameter of the tube (Figure 2B). To distinguish different cell types, we stained the HUVECs, SMCs, and HAFs with different fluorescent dyes (HUVECs, CellTracker violet; SMCs, CellTracker green; HAFs, CellTracker deep red) before seeding them into the microfluidic chip. After 1-day incubation in culture medium (DMEM, 10% fetal bovine serum FBS, 37°C, 5% CO_2), cells were attached to the MPC-PLC membrane (Figures 2D and 2H). We peeled the microfluidic chip off the cell-laden MPC-PLC membrane and rolled

Please cite this article in press as: Cheng et al., Electronic Blood Vessel, Matter (2020), https://doi.org/10.1016/j.matt.2020.08.029

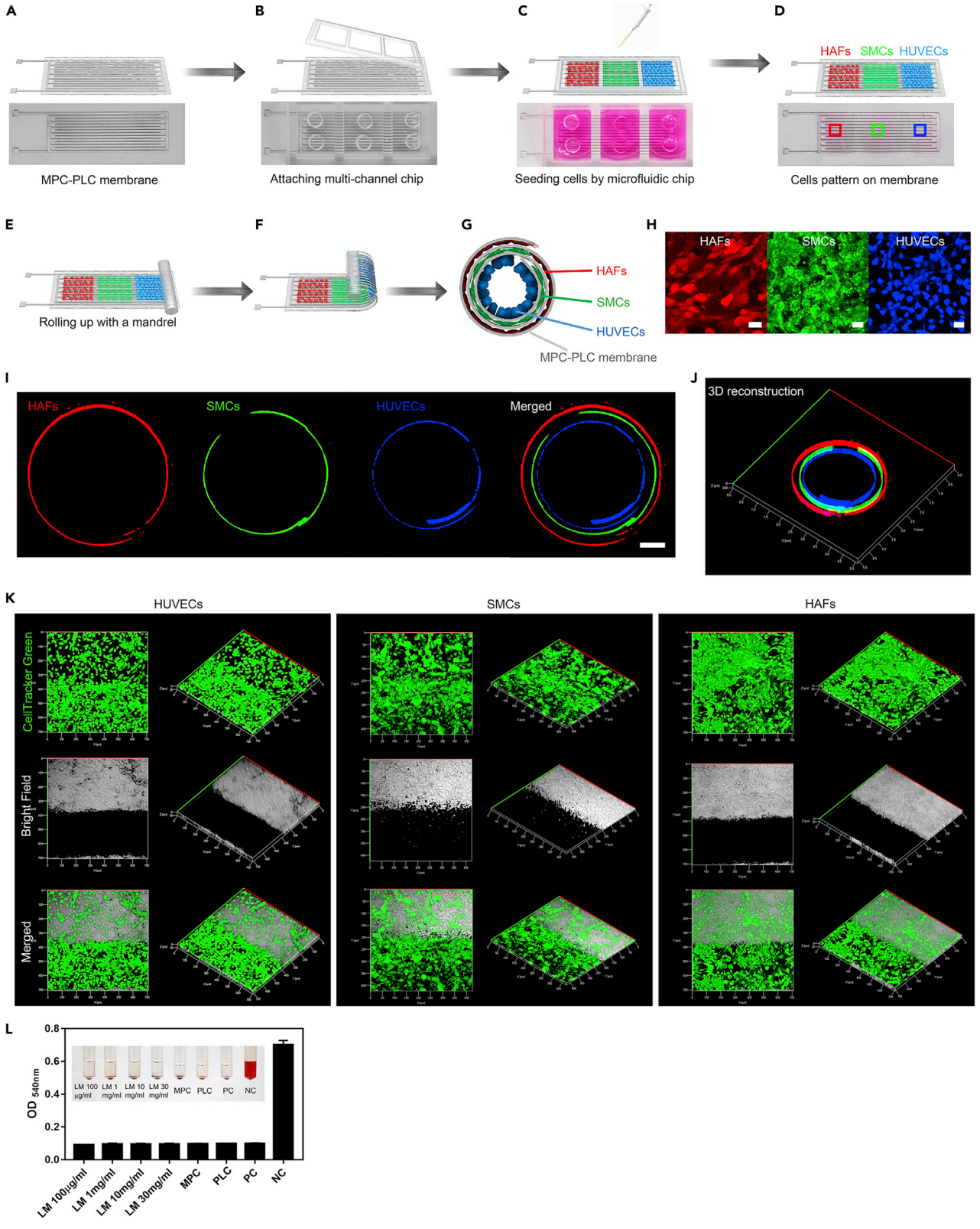

Please cite this article in press as: Cheng et al., Electronic Blood Vessel, Matter (2020), https://doi.org/10.1016/j.matt.2020.08.029

Figure 2. *In Vitro* Biocompatibility of the Electronic Blood Vessel

(A) The MPC-PLC membrane.

(B) Attaching a multichannel microfluidic chip onto the MPC-PLC membrane.

(C and D) Patterning three kinds of blood-vessel cells (blue, HUVECs; green, SMCs; red, HAFs) onto the MPC-PLC membrane using a polydimethylsiloxane microfluidic chip. (C) Seeding the cells. (D) Cell pattern.

(E and F) Rolling the cell-laden membrane into a multilayered tubular structure with a PTFE mandrel. (E) Step 1. (F) Step 2.

(G) Cross-sectional view of natural-blood-vessel-mimicking structure with different cells distributed in different layers.

(H) Fluorescence images of cells on the MPC-PLC membrane, corresponding to (D). Stained by CellTracker violet, green, and deep red. Scale bar, 20 μm.

(I) Three kinds of blood-vessel cells distributed in different layers of the electronic blood vessel. Scale bar, 500 μm.

(J) 3D construction of (I).

(K) Cell viability after 2-week incubation in the electronic blood vessel. Stained by CellTracker green. The right column is the 3D reconstruction of the left column in each image. The black area represents the MPC circuit and the transparent area represents the PLC in bright-field images.

(L) Hemolysis test. The MPC circuit, PLC membrane, and liquid metal with different concentrations were tested with rabbit whole blood and exhibited good blood compatibility. Saline was used as the positive control (PC), whereas water was used as the negative control (NC).

it up with a PTFE mandrel, forming a 3D multilayered tubular structure (Figures 2E–2G) with HUVECs, SMCs, and HAFs evenly distributed in the inner layer, middle layer, and outer layer, respectively (Figures 2I and 2J). This structure mimics well the structure of the natural blood vessel. To better understand the blood-vessel cells distributed in the different layers of the electronic blood vessel, we stained HUVECs, SMCs, HAFs, and the MPC-PLC layer with CellTracker DiO, CellTracker DiI, CellTracker DiD, and CellTracker blue to show the relative distribution of the different layers (Figure S3). We used a biomedical fibrin glue to facilitate the combination of the different layers.[18] We incubated the cell-laden electronic blood vessel for 14 days and stained the cells with calcein-AM green. The evenly distributed green color on the MPC-PLC membrane indicated that the cells exhibited high viability after a 14-day culture (Figure 2K). We measured the transport of ions through the MPC-PLC membrane to further evaluate and quantify the permeability of the electronic blood vessel (Figure S4). Ca^{2+}, Fe^{3+}, and Mg^{2+} could permeate the electronic blood vessel over time. We also conducted a hemolysis test, which showed that the electronic blood vessel exhibited very good blood biocompatibility (Figure 2L). The *in vitro* characterization demonstrated that the electronic blood vessel exhibited excellent biocompatibility, and we then conducted further functional tests of the embedded MPC circuits, i.e., electrical stimulation and electroporation.

In Vitro Electrical Stimulation Promotes HUVEC Proliferation and Migration

To prove the functionality of the electronic blood vessel, we carried out *in vitro* electrical stimulation to improve proliferation and migration of HUVECs. A direct current (DC) electric field has been shown to effectively increase angiogenesis *in vitro* and *in vivo*.[26] We patterned HUVECs on the MPC-PLC membrane (DMEM, 10% FBS, 37°C, 5% CO_2) by using a multichamber polydimethylsiloxane (PDMS) chip. The initial number of cells in each chamber was the same (3×10^4). After 12-h incubation, we applied different DC voltages to yield different electrical field strengths: 25, 50, 75, 100, 200, and 400 mV mm^{-1} (Figures 3A and 3B). After 2-day incubation and electrical stimulation, we randomly selected six different domains on each sample and analyzed them by using laser scanning confocal microscopy (LSM 710, Zeiss, Germany). We stained nuclei (blue) with Hoechst 33342 (Invitrogen, USA) and stained the living and dead cells with calcein-AM (green) and propidium iodide (PI) (red), respectively. The green cells occupied the whole domain, indicating that electrical stimulation did not hurt the proliferation of HUVECs (Figure 3C). We counted the nuclei using ImageJ. The cell number under 50 mV mm^{-1} was highest, about 2.4 times that of the control (Figure 3E). We used the CCK-8 kit to confirm this conclusion (Figure 3F). We speculated that the DC electric field had selectively regulated the production of certain growth factors and cytokines important for angiogenesis.

Please cite this article in press as: Cheng et al., Electronic Blood Vessel, Matter (2020), https://doi.org/10.1016/j.matt.2020.08.029

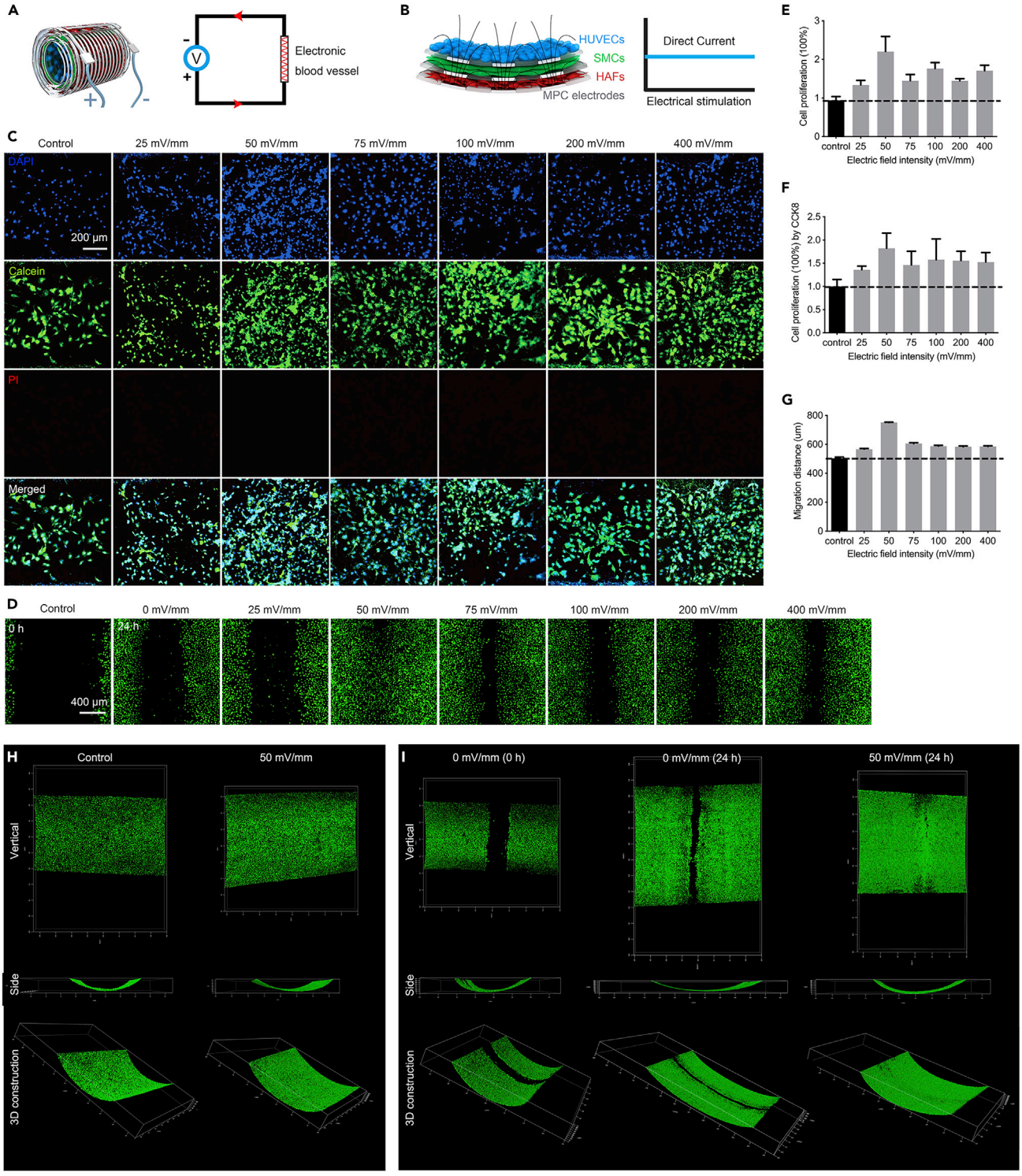

Figure 3. *In Vitro* Electrical Stimulation

(A and B) The electronic blood vessel was connected to an electrochemical station (A) to generate a DC voltage (B).

(C) Confocal fluorescence images of HUVEC proliferation after 2-day incubation and stimulation under different DC electric fields: 25, 50, 75, 100, 200, and 400 mV/mm. Blue, DAPI; green, calcein-AM; red, PI. Scale bar, 200 μm.

(D) Confocal fluorescence images of HUVEC migration after 24-h incubation and stimulation under different DC electric fields: 25, 50, 75, 100, 200, and 400 mV/mm. Stained by calcein-AM. Scale bar, 400 μm. A 10-μL tip was used to scratch a line to create a model for HUVEC migration.

Please cite this article in press as: Cheng et al., Electronic Blood Vessel, Matter (2020), https://doi.org/10.1016/j.matt.2020.08.029

Figure 3. *Continued*

(E) The proliferation of HUVECs under different DC electrical fields, setting the control (without electric field) as 100% (n = 4).

(F) The proliferation of HUVECs under different DC electrical fields tested with the CCK-8 kit (n = 4).

(G) The migration of HUVECs at different DC electrical fields (n = 4).

(H) The proliferation of HUVECs in a 3D model under a DC electric field of 50 mV/mm. Stained by calcein-AM.

(I) The migration of HUVECs in a 3D model under a DC electric field of 50 mV/mm. Stained by calcein-AM. The HUVECs formed a complete endothelial layer after 24-h electrical stimulation.

We explored the migration of HUVECs under different DC electric field strengths. We made a scratch on a PDMS substrate using a 10-μL tip. After application of an electric field of 50 mV mm^{-1}, HUVECs migrated 750 μm and the wound completely healed after 24 h (Figure 3D). Different strengths enhanced migration differently compared with the control group without electrical stimulation (Figure 3G). The *in vitro* DC electrical stimulation thus proved to have effectively promoted the proliferation and migration of HUVECs.

We further evaluated the effectiveness of electrical stimulation in a 3D model of endothelialization. We patterned the HUVECs on the MPC-PLC membrane and made a scratch on the cell-laden membrane using a 10-μL tip. We transformed the 2D cell-laden membrane into a 3D cell-laden structure and connected it to the electrochemical station to test the proliferation and migration. We applied an electric field of 50 mV mm^{-1} on multiple samples and we observed the proliferation and migration at different time points. We stained the living and dead cells with calcein-AM (green) and PI (red). We counted the cells and the cell density was higher than that of the control group (Figure 3H). The HUVECs formed a complete endothelial layer after 24 h (Figure 3I). To better evaluate the biocompatibility of the MPC circuit under electrical stimulation, we extended the electrical stimulation time to 10 days, and the live/dead staining showed that cells exhibited excellent viability (Figure S5).

In Vitro Electroporation

To further prove the functionality of the electronic blood vessel, we designed multiple circuit patterns for electroporation, being able to target different pathological issues in different layers of blood-vessel cells (Figure S1B). We conducted the electroporation with a circuit pattern that could target all three layers. We seeded the cells onto the MPC-PLC membrane and transformed it into a 3D tubular structure for electroporation. We immersed the 3D cell-laden electronic blood vessel in the GFP plasmid DNA solution for 10 min before electroporation. The GFP plasmid DNA could also be lyophilized onto the MPC-PLC membrane before seeding cells (Figure S7A) and transforming to the 3D structure for electroporation. We connected the 3D cell-laden electronic blood vessel to an electroporator (BTX, CM630, US) to generate DC pulses (Figure 4A) and achieved delivery of the GFP DNA plasmid in the three kinds of blood-vessel cells (Figure 4B). To optimize the performance of the electronic blood vessel, we found two major parameters determining the efficacy of electroporation, including voltage and pulse duration. We conducted the electroporation with different voltages (40/60/80 V) and pulse durations (100 μs/1 ms). If the voltage was too low, it would cause low efficacy or no transfection; if the voltage was too high or if the pulse duration was too long, it would cause low efficacy and cell death (Figure S6). To realize the optimal efficacy, we exerted a square wave with a voltage of 60 V, pulse duration of 100 μs, and pulse interval of 1 s for five pulses. We delivered the GFP plasmid DNA into three kinds of blood-vessel cells and the GFP DNA realized expression with more than 95% of cells showing green fluorescence (Figure 4B). We observed successful expression of GFP among all three layers of the blood-vessel cells and they exhibited a uniform 3D distribution in the electronic blood vessel (Figure 4C). To evaluate the potential of the electronic blood

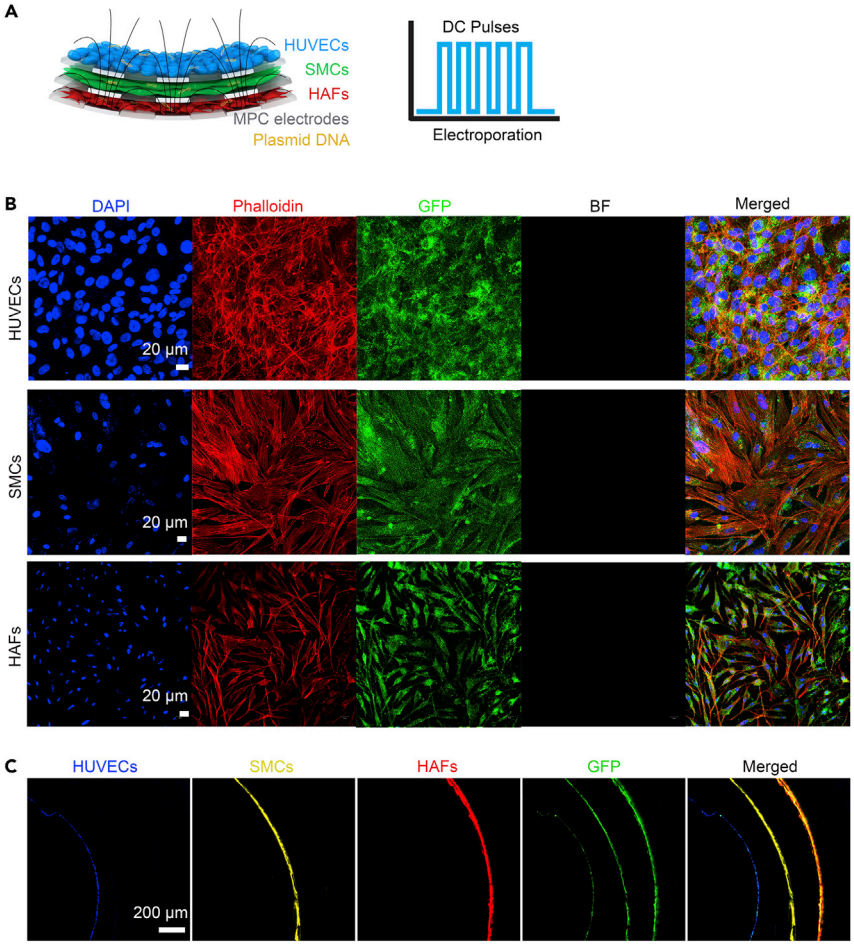

Figure 4. *In Vitro* Electroporation

(A) The electronic blood vessel was connected to an electroporator to generate electrical pulses. (B) Confocal fluorescence images of HUVECs, SMCs, and HAFs after electroporation under the following conditions: voltage 60 V; pulse duration 100 μs; five pulses; pulse interval 1 s. Top, HUVECs; middle, HAFs; bottom, SMCs. Blue represents cell nucleus, stained by DAPI; red represents cell skeleton, stained by rhodamine phalloidin; green represents GFP; black represents cells that were on the top of the non-transparent MPC-PLC circuit; bright field. Scale bar, 20 μm. (C) The 3D distribution of HUVECs, SMCs, and HAFs after electroporation under the following conditions: voltage 60 V; pulse duration 100 μs; five pulses; pulse interval 1 s. Blue represents HUVECs, stained by CellTracker blue; yellow represents SMCs, stained by CellTracker DiI; red represents HAFs, stained by CellTracker DiD; green represents green fluorescent protein. Scale bar, 200 μm.

vessel for *in vivo* electroporation, we lyophilized the GFP plasmid DNA on the MPC-PLC membrane to test its effectiveness (Figure S7A). We carried out electroporation by attaching the plasmid-laden MPC-PLC membrane to an isolated rabbit vascular tissue with a voltage of 60 V, pulse duration of 100 μs, and pulse interval of 1 s for five pulses. We observed successful expression of GFP in the isolated rabbit vascular tissue (Figure S7B) after a 2-day incubation. These promising *in vitro* results encouraged us to carry out *in vivo* tests on the electronic blood vessel.

Mechanical Properties of the Electronic Blood Vessel

To find out whether the electronic blood vessel is suitable for *in vivo* implantation, we measured the mechanical properties, including stress-strain curve, compliance,

Please cite this article in press as: Cheng et al., Electronic Blood Vessel, Matter (2020), https://doi.org/10.1016/j.matt.2020.08.029

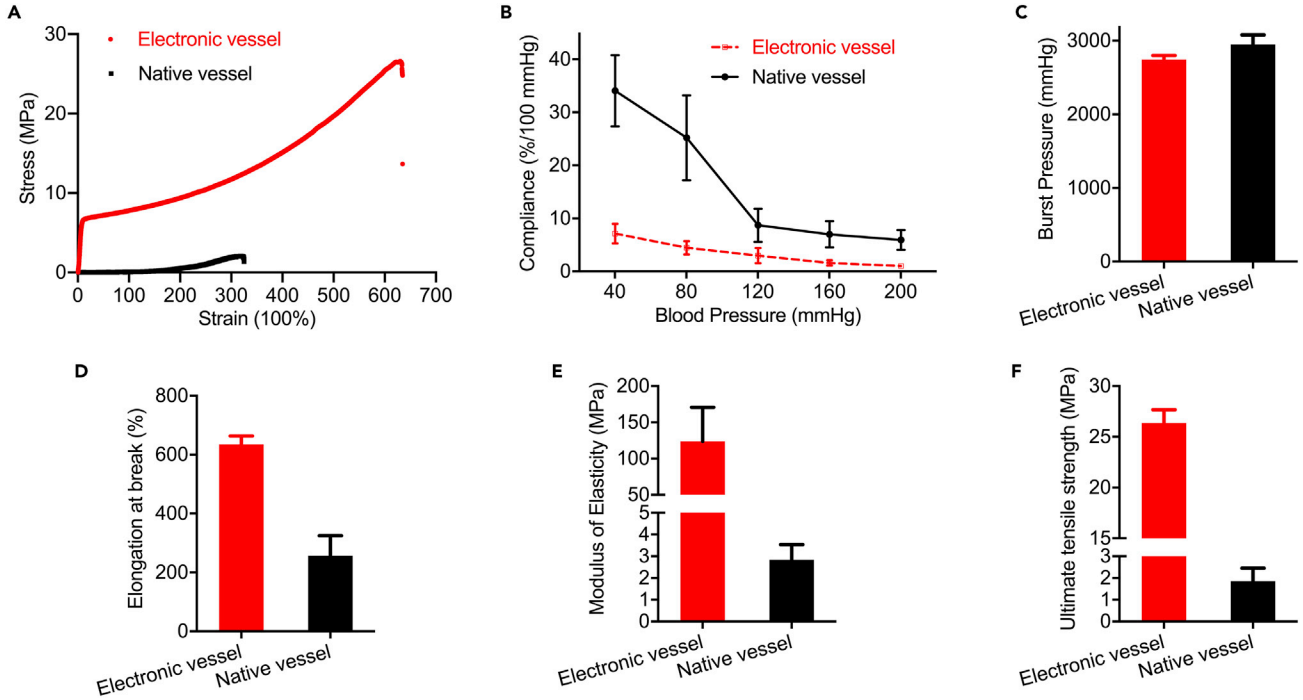

Figure 5. Mechanical Properties of the Electronic Blood Vessel

(A) Stress-strain curve.

(B) Compliance test.

(C) Burst pressure test.

(D) Elongation at break.

(E) Modulus of elasticity.

(F) Ultimate tensile strength. Electronic blood vessel (n = 5) and native carotid artery (n = 3) were used in each test. All data are expressed as the mean ± SD.

and burst pressure, of the electronic blood vessel with a diameter of 2 mm prior to implantation (Figures 5A–5F and S8). The elastic modulus of the electronic blood vessel is about 130 MPa; this value is much higher than that of the native carotid artery. The ultimate tensile strength of the electronic blood vessel is about 27 MPa; this value is also much higher than that of the native carotid artery. The initial compliance of the electronic blood vessel (n = 5) is about 5% per 100 mm Hg in the range of 80–120 mm Hg; this value is apparently below that of the native carotid artery (n = 3). The burst pressure of the electronic blood vessel (n = 5) is about 2,800 mm Hg; this value is similar to that of the native carotid artery (n = 3). The elongation at break of the electronic blood vessel is about 650% (n = 5), which is twice the value of the native carotid artery (n = 3). The mechanical properties of the electronic blood vessel were considered robust enough for implantation.

In Vivo Implantation in Rabbits and *In Situ* Monitoring

To investigate the electronic blood vessel as a vascular implant, we chose the New Zealand rabbit (age, 200–300 days; body weight, 3–4 kg) as the animal model and replaced the native carotid artery with the electronic blood vessel (Figures 6A–6C). To avoid possible immunological response of the host tissue, we used the acellular electronic blood vessel in the preliminary *in vivo* study. We monitored the implanted electronic blood vessel *in situ* by Doppler ultrasound imaging (Figures 6D–6I) and arteriography (Figures 6J and 6K). Doppler ultrasound imaging showed that the electronic blood vessel allowed for good blood flow 3 months post-implantation (Figures 6D–6G and Video S1). The asymmetric velocity curve synchronized with the ultrasonic pulses

Please cite this article in press as: Cheng et al., Electronic Blood Vessel, Matter (2020), https://doi.org/10.1016/j.matt.2020.08.029

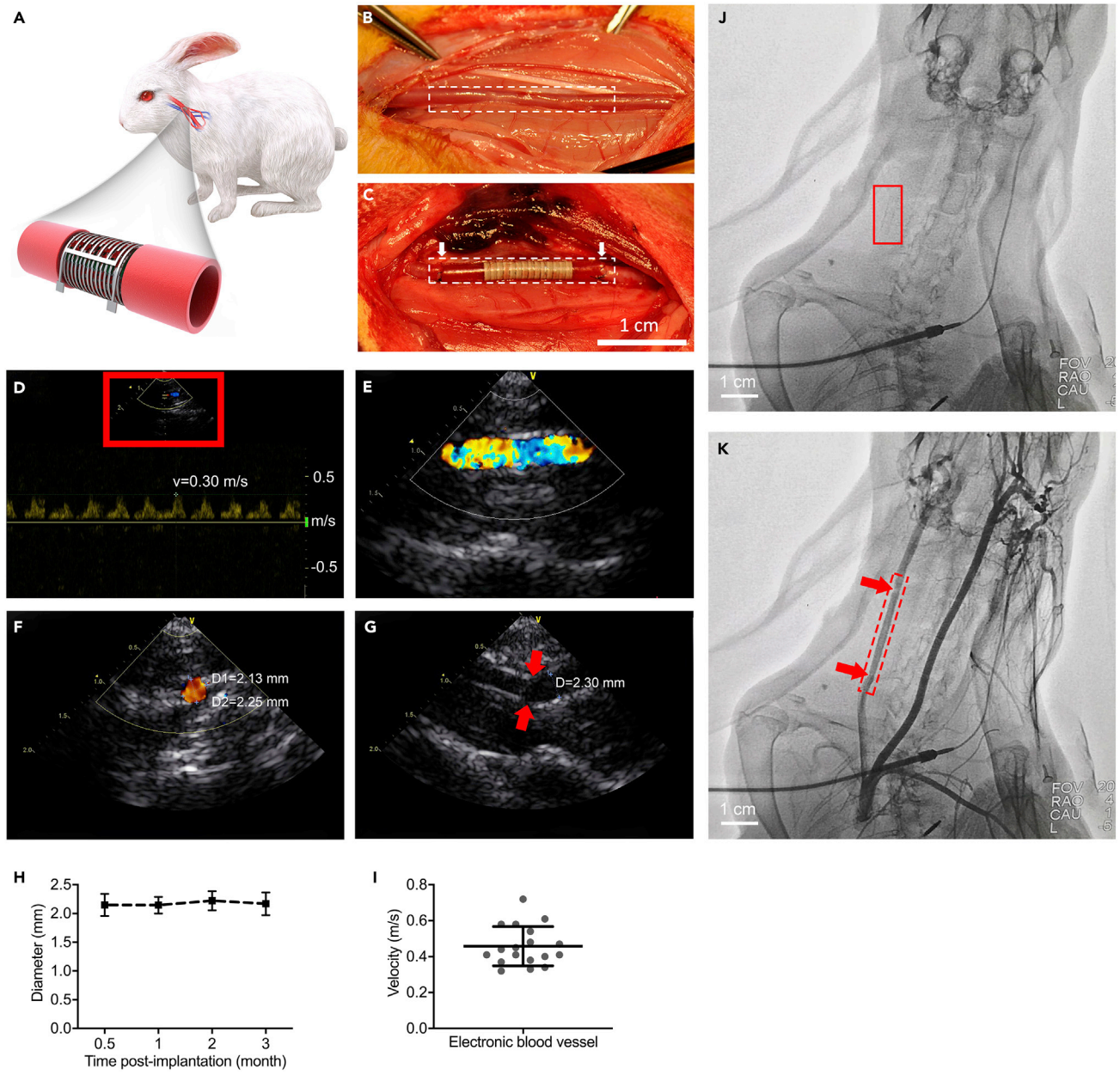

Figure 6. *In Situ* Monitoring of the Electronic Blood Vessel

(A) Schematic of the electronic blood vessel in the carotid artery of the rabbit.

(B and C) An end-to-end anastomosis procedure of electronic blood vessel implantation in carotid arteries of rabbits (n = 6). The dotted frames (B and C) outline the margin of the native carotid artery and the implanted electronic blood vessel. The white arrows (C) indicate the two ends of the electronic blood vessel. Scale bar, 1 cm.

(D–G) *In situ* monitoring of the electronic blood vessel by Doppler ultrasound imaging 3 months post-implantation. Representative images from at least three different animals. (D and E) The real-time blood flow at the operational site and the synchronized ultrasound pulses. The asymmetric velocity curve indicates that the signal is from the carotid artery rather than the vein. (E) Zoom-in view of red box in (D). (F) The cross-sectional view of the blood flow. (G) The suture site (red arrows) connecting the native carotid artery and the electronic blood vessel.

(H) The diameter changes in the electronic blood vessel at different times post-implantation.

(I) The velocity of blood flow at the operational site (n = 18, from different rabbits at different time points).

(J and K) *In situ* monitoring by arteriography 3 months post-implantation. (J) Image before injecting the contrast medium. Red box indicates the position of the implanted electronic blood vessel. Scale bar, 1 cm. (K) Image after injecting the contrast medium. Red box indicates the position of the implanted blood vessel. Red arrows indicate the suture sites connecting the native carotid artery and the electronic blood vessel. Scale bar, 1 cm.

indicated that the signal is from the carotid artery rather than the vein (Figure 6D). The diameter of the electronic blood vessel remained at a relatively constant value, about 2.3 mm, during the half-month to 3 months post-implantation (Figures 6G and 6H). The mean velocity of the blood flow in different samples at different time points was about 0.47 m s^{-1}, which was in the range of the normal value (Figure 6I). As the gold standard of the blood-vessel patency, arteriography showed that the electronic blood vessel matched the native carotid artery very well and allowed for excellent blood flow (Figures 6J, 6K, and S9, and Video S2). There was no sign of narrowing. The electronic blood vessel allows straightforward visualization under arteriography because the liquid metal-based circuitry has sufficiently high contrast over host tissues (Figure 6J). The red frame in the figure outlines the electronic blood vessel with an alternate strip structure from the MPC circuit.

Ex Vivo Study

We dissected all the implanted electronic blood vessels 3 months post-implantation for characterization. The lumen and the outer surfaces of the explanted electronic blood vessel were smooth, covered by the remodeling tissues (Figures 7A and 7B). The diameter of the native blood vessel was significantly reduced due to the lack of blood pressure, whereas the electronic blood vessel remained the same as before (Figure 7C). We observed the microstructure of the circuit by scanning electron microscopy (SEM) after explanting the electronic blood vessel from the rabbit. The MPC-PLC membrane still maintained interdigitated structure with the MPC circuit and PLC host (Figure 7E). There was a layer of neo-tissue formed, which well covered the MPC-PLC membrane (Figures 7F–7H). We could also see some red blood cells on the top of the circuits, which were similar in number to those on native blood vessels (Figure 7D). We tested the conductivity of the circuit in the electronic blood vessel. The MPC circuit was still conductive and the conductivity was around 7.2×10^3 S cm^{-1}.

To study the histological changes in the implanted electronic blood vessels, we performed histological staining of the electronic blood vessels, setting the native carotid blood vessel as a positive control. H&E staining (Figure 7I) of the cross section of the electronic blood vessel showed it as round shaped, continuous, and red, which is similar to the native blood vessel. The three-layered MPC-PLC membrane merged into one intact layer with secretion of a substantial extracellular matrix between the different layers of electronic blood vessel. We could clearly see dark blue nuclei (red arrows in Figure 7I) in all the layers, which indicated successful migration and infiltration of host cells into the electronic blood vessel. We compared the cell density in the electronic blood vessel with the native carotid. The cell density of the electronic blood vessel was around 400 cells mm^{-2}, whereas that of the native carotid was around 535 cells mm^{-2}. More importantly, a dense layer of cells with curved structure was formed in the lumen of the electronic blood vessel, which indicated the excellent endothelialization and thus ensured good blood flow. To further confirm the components in the implanted electronic blood vessel, we performed Masson's trichrome (Figure 7J) and Verhoeff's staining (Figure 7K). Masson's trichrome can stain and assess keratin and muscle fibers (red) or collagen (blue) and Verhoeff's can stain and assess the presence of elastin fibers. Masson's trichrome and Verhoeff's staining showed well-distributed collagen and elastin fibers both inside the layers and between different layers, indicating appropriate remodeling. Compared with the abundance level of extracellular matrix in the native blood vessel, the electronic blood vessel still requires more time for material degradation and tissue remodeling. These results indicated that the electronic blood vessel might still be functioning in the presence of conductive materials and host remodeling 3 months post-implantation.

Please cite this article in press as: Cheng et al., Electronic Blood Vessel, Matter (2020), https://doi.org/10.1016/j.matt.2020.08.029

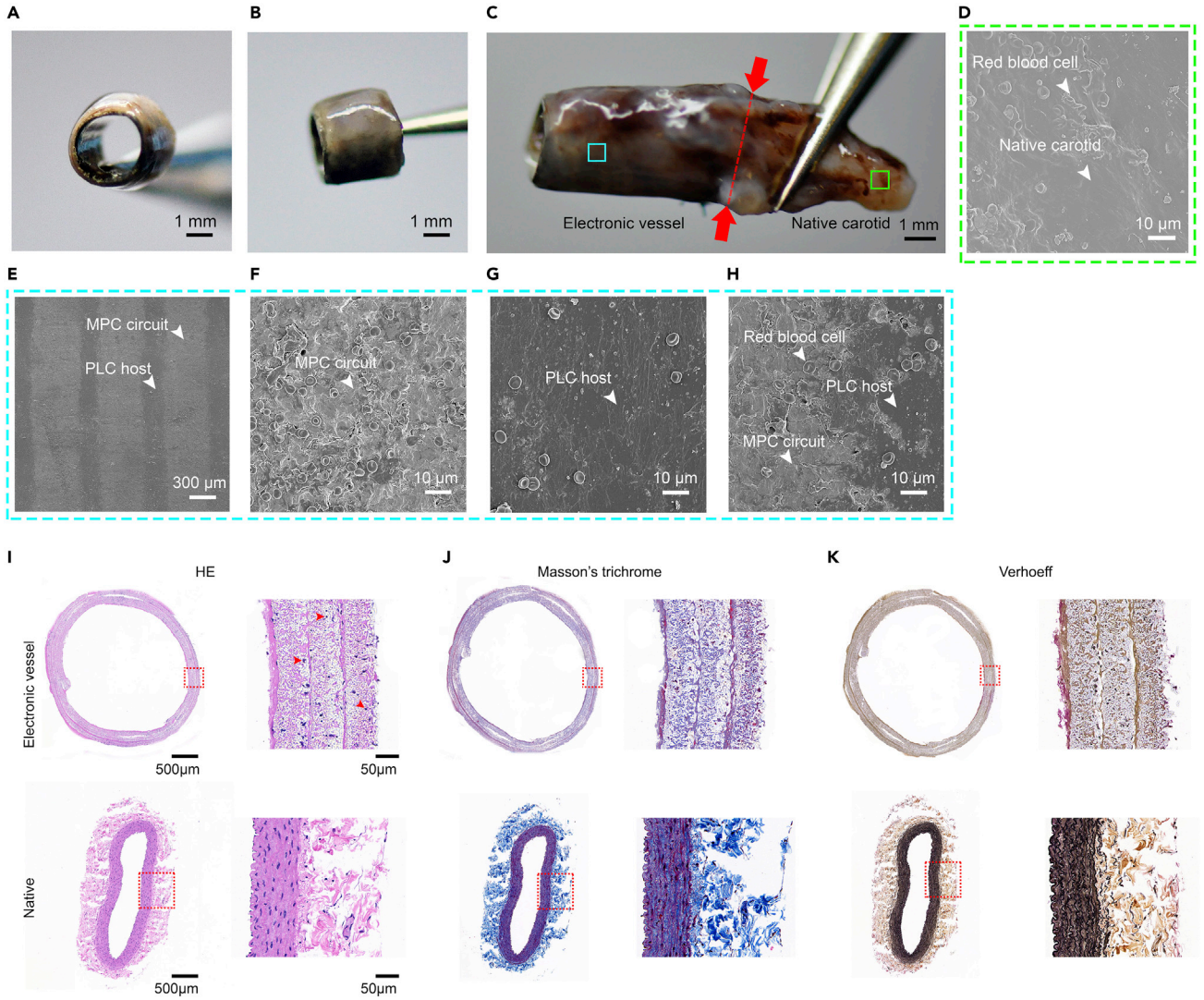

Figure 7. *Ex Vivo* Study of the Electronic Blood Vessel after 3 Months Implantation in the Rabbit

(A–C) The cross-sectional (A) and lateral views (B and C) of the explanted electronic blood vessel after 3 months of host remodeling. Red arrows and the dotted line indicate the suture site connecting the native carotid artery (right) and the electronic blood vessel (left). Scale bar, 1 mm.

(D) Representative SEM image of the lumen of the native carotid. Scale bar, 10 μm.

(E) Representative SEM image of the lumen of the electronic blood vessel. Scale bar, 300 μm.

(F–H) Zoom-in views of the MPC circuit (F), PLC host (G), and interconnection area of the MPC circuit and PLC host (H). Scale bar, 10 μm.

(I–K) Hematoxylin/eosin (HE) staining (I), Masson's trichrome staining (J), and Verhoeff's staining (K) of the implanted electronic blood vessel 3 months post-implantation, setting the native carotid artery as control. The right image is the zoom-in view of the left. Scale bar (left), 500 μm. Scale bar (right), 50 μm.

To investigate the influence of the electronic blood vessel on the host, we performed cross-sectional and histological staining of the major organs, including heart, liver, spleen, lung, and kidney, together with dissection of the implanted electronic blood vessel 3 months post-implantation. The H&E staining and Masson's Chrome staining showed that there were no significant pathological changes or inflammatory responses in these organs (Figure S10). To evaluate whether there was chronic inflammation or infection, we conducted ELISA on three important proteins in the blood, comprising interleukin-6 (IL-6), procalcitonin (PCT), and C-reactive protein (CRP) (Figure S11). The concentrations of IL-6 and PCT were not higher than the normal value of healthy rabbits (red dotted lines in the figure). The concentration of CRP

Please cite this article in press as: Cheng et al., Electronic Blood Vessel, Matter (2020), https://doi.org/10.1016/j.matt.2020.08.029

was higher than the normal value of healthy rabbits (red dotted line). All three indexes decreased over time, a tendency that was expected. The results showed that most of the indexes were in the normal range and there were no significant pathological changes or inflammatory responses. We also conducted a complete blood count of the rabbit, including white blood cell count, absolute neutrophil count, and absolute lymphocyte count, most of which were in the normal range over time (Figure S12). These results confirmed that as an implant for vascular system, the electronic blood vessel had no significant detriment to the host.

DISCUSSION

None of the existing small-diameter TEBVs has met the demands of treating cardiovascular diseases. Conventional TEBVs can be greatly improved to provide next-generation treatment by integrating with flexible bioelectronics. In this work, we report an electronic blood vessel with excellent biocompatibility, flexibility, mechanical strength, and degradability by combining MPC with a US FDA-approved biodegradable polymer. As a proof of concept, we verified that the electronic blood vessel can accelerate HUVEC proliferation and migration by electrical stimulation, thus facilitating the endothelialization process, which is important to an engineered vascular conduit in preventing early thrombosis. Because most TEBVs occluded by 2 weeks post-implantation, our electronic blood vessel, with a patency of at least 12 weeks, is of great promise for clinical application. We also showcase that it could be used to perform *in situ* gene delivery via electroporation, which laid the foundation for future design and optimization such that we can carry out further gene therapies targeting different pathological problems after implantation.

The electronic blood vessel has a high level of safety. The liquid metal[16,27] has been proven to be highly biocompatible and the PLC has been approved by the US FDA for implants.[28] We validated its biosafety in the vascular system by a 3-month implantation in a rabbit carotid artery model. Both the *in situ* monitoring, including Doppler ultrasound imaging and arteriography, and the *ex vivo* study demonstrated that it was safe as an electronic implant in the vascular system and at the body level. The electronic blood vessel exhibited higher strength than the native blood vessel. The potential harm of a rigid synthetic blood vessel is the mismatch with host tissue after implantation. However, from the *in vivo* results, these discrepancies did not bring about any major issues, and the electronic blood vessel matched very well with the host carotid artery during the time of *in situ* monitoring (Figures 6J and 6K, Video S2). The reasons we chose liquid metal in the electronic blood vessel are as follows: (1) compared with gold or platinum, the Ga-In liquid metal allows superior flexibility and stretchability while maintaining good conductivity, which is critical for an artificial blood vessel to adapt to the deformation due to rhythmic beating; (2) it exhibits excellent cytocompatibility and blood compatibility according to our results; and (3) compared with other sophisticated microfabrication techniques, using the screen-printing technique is much more straightforward and could enable industrial-scale mass production in a cost-effective manner.

As a vascular substitute, the electronic blood vessel breaks through the limitations of the existing vascular scaffold by endowing the electrical function on a conventional biodegradable TEBV and provides us a new platform for tackling the problems threatening the small-diameter blood vessel. By integrating with other electronic devices, the electronic blood vessel can provide various treatments, such as electrical stimulation, electroporation, electrically controlled drug release, and so forth. When combined with emerging technologies such as artificial intelligence, it can greatly boost

future personalized medicine by bridging the vascular tissue-machine interface and empowering health data collection and storage, such as blood velocity, blood pressure, and blood glucose level. In the future, optimizing its function and creating a multifunctional electronic blood vessel can greatly benefit human cardiovascular health.

Conclusions

In this work, by integrating liquid metal-based conducting circuitry with a biodegradable polymer, we develop an electronic blood vessel, with excellent biocompatibility, flexibility, conductivity, mechanical strength, and degradability, that enables *in situ* electrical stimulation to facilitate the endothelialization process and electroporation to deliver genes into specific layers of blood-vessel cells. It exhibited excellent patency and biosafety 3 months post-implantation in the vascular system of a rabbit model. In the future, the electronic blood vessel can be integrated with other electronic components and devices to enable diagnostic and therapeutic functions and greatly empower personalized medicine by creating a direct link in the vascular tissue-machine interface.

EXPERIMENTAL PROCEDURES

Resource Availability

Lead Contact

Further information and requests for resources and reagents should be directed to and will be fulfilled by the lead contact, Xingyu Jiang (jiang@sustech.edu.cn).

Material Availability

All materials generated in this study will be made available on request, but we may require a payment and/or a completed materials transfer agreement if there is potential for commercial application.

Data and Code Availability

All data are available from the lead contact upon reasonable request. This study did not generate any code.

Preparation of the Liquid Metal Conductive Ink

We added 2.5 g EGaIn (gallium indium eutectic, 99.99%, Sigma-Aldrich) to 1 mL 1-decanol (98%, Macklin, China). We sonicated the mixture for 1 min at a power of 300 W using a sonicator (Scientz-IID, Scientz, China). We obtained a solution of LMPs of 2.5 g mL^{-1} and we used it as the conductive ink for screen-printing.

Preparation of MPC-PLC Membrane

We used a screen-printing apparatus (Taobao, China) and employed a PET membrane (Taobao, China) as the substrate for screen-printing. We screen-printed the conductive liquid metal ink onto a screen-printing template (Taobao, China) with the desired pattern. We dissolved the PLC (70:30, RESOMER, Evonik, Germany) particles in dichloromethane (CH_2Cl_2) at 5 wt% to prepare the PLC solution. After evaporation of the 1-decanol in an oven at 80°C for 10 min or at room temperature for 2 h, we embedded the LMP circuit into the PLC solution. After evaporation of CH_2Cl_2 at room temperature for 12 h, we peeled the MPC-PLC membrane off the PET substrate.

Characterization of the MPC-PLC Membrane

We observed the morphology of the LMPs and the MPC-PLC membrane by SEM (SU8220, Hitachi, Japan) and transmission electron microscopy (T20, FEI, USA). The LMPs inside the PLC membrane were fully degraded and removed by adding excessive hydrochloric acid (Beijing Chemicals Works, China) and rinsing with ultrapure water

Please cite this article in press as: Cheng et al., Electronic Blood Vessel, Matter (2020), https://doi.org/10.1016/j.matt.2020.08.029

(Thermo Fisher Scientific, USA) more than three times. We analyzed the diameter of the LMPs using ImageJ (NIH, USA). We bent the MPC-PLC membrane 180° for 1,000 cycles and measured the conductivity after each 250 cycles and normalized the resistance value to the initial value. For the degradation test, we incubated the MPC-PLC membrane (n = 48) in a PBS solution (pH 7.4, 37°C, 5% CO_2) for 8 weeks and refreshed the PBS solution every day. In the first week, we took out three samples every day and afterward we took out three samples every week, washed them with ultrapure water more than three times, removed the residual water by using a lyophilizer (FD-1A-50, Biocool, China), and tested the weight and analyzed the mass loss.

Permeability of MPC-PLC Membrane

We used a 70-μm MPC-PLC membrane folded in half to wrap the 2-mL solution, which contained 2.4 mg mL^{-1} Mg^{2+}, 2 mg mL^{-1} Fe^{3+}, and 2.3 mg mL^{-1} Ca^{2+}, as the sample to measure the permeability of these cations. The whole piece was sealed by dialysis clamps and put in a beaker filled with 400 mL deionized water for 18 days. We measured the concentrations of these cations in the beaker at 2, 5, 10, and 18 days by inductively coupled plasma mass spectrometry (Agilent 7700×, USA), and set the initial deionized water as the control group.

Preparation of the MPC-PLC Electronic Blood Vessel

We prepared the MPC-PLC electronic blood vessel by rolling up the MPC-PLC membrane with the assistance of a PTFE mandrel (Taobao, China). The diameter of the PTFE mandrel was 1.8 mm. We used a biomedical fibrin glue (Fibrin Sealant Kit, Puji Medical Technology Development Co., Ltd, Hangzhou, China) to facilitate the combination of different layers.

Cell Patterning

We sterilized the MPC-PLC membrane by radiation with a cobalt radiation device (Co 60, 10–130 Gy min^{-1}, Peking University, China). Before cell seeding, the MPC-PLC membrane was incubated with fibronectin solution (50 μg mL^{-1}) for 6 h at room temperature to facilitate the cell attachment. We deployed a PDMS chip with three channels to seed three kinds of blood-vessel cells, HUVECs (ATCC, USA), SMCs (ATCC, USA), and fibroblasts (ScienCell, USA), on the surface of the MPC-PLC membrane. After overnight incubation, we removed the PDMS chip from the cell-laden MPC-PLC membrane and rolled the cell-laden MPC-PLC membrane into a natural-blood-vessel-mimicking tubular structure with the assistance of a PTFE mandrel. The three kinds of blood-vessel cells were distributed in different layers of the electronic blood vessel sequentially, i.e., HUVECs (inner layer), SMCs (middle layer), and fibroblasts (outer layer). To deliver different cells to different layers accurately, we designed the width of each channel according to the circumference of the corresponding layers. We cultured the cell-laden MPC-PLC membrane and the MPC-PLC electronic blood vessel in DMEM supplemented with 10% FBS (5% CO_2, 37°C). To image the cells, we stained the HUVECs (blue), SMCs (green), and fibroblasts (red) with CellTracker violet, green, and deep red (Life Technologies, USA), respectively. We used a confocal laser scanning microscope (CLSM; LSM710, Zeiss, Germany) to capture the fluorescent images.

Cytotoxicity of the MPC-PLC Electronic Blood Vessel

We cultured the MPC-PLC electronic blood vessel for 2 weeks. We used calcein-AM green to test the viability of the cells embedded in the MPC-PLC electronic blood vessel. We washed the cell-laden electronic blood vessel with fresh PBS solution three times and incubated it in calcein-AM green solution at a concentration of 5 μL mL^{-1} for 20 min. After three washes with PBS, we fixed the cells with

4% paraformaldehyde aqueous solution for 10 min. We used CLSM (LSM710, Zeiss, Germany) to capture the fluorescent images. We took the multilayered images of the sample and performed 3D reconstruction of the cells using ZEN software (Zeiss, Germany). We re-spread the electronic blood vessel before taking image.

Hemolysis Test

We extracted fresh rabbit blood into an anticoagulant tube and centrifuged at 1,500 rpm for 10 min. We collected the erythrocytes after three washes with saline. We prepared LMPs in saline at different concentrations, 5 mg PLC membrane, and 5 mg PLC-MPC membrane. We mixed the samples with the erythrocytes. The final hematocrit level of red blood cells was about 4%. After 4-h incubation at 37°C, we extracted the supernatant after centrifugation at 12,000 rpm for 10 min and measured the absorbance at 540 nm by UV-Vis analysis. We used saline as the negative control and pure water as the positive control.

Cell Proliferation by *In Vitro* Electrical Stimulation

To evaluate proliferation by electrical stimulation, we patterned HUVECs on the MPC-PLC electronic blood vessel and incubated overnight in DMEM supplemented with 10% FBS (5% CO_2, 37°C). We connected the MPC-PLC electronic blood vessel to a multichannel electrochemical station (1040C, CHI, China) to generate DC. We connected six samples to separate channels with different voltage outputs, setting a sample without electrical stimulation as control. We generated electrical fields of 25, 50, 75, 100, 200, and 400 mV mm^{-1} by exerting a voltage of 25, 50, 75, 100, 200, and 400 mV, respectively. The interval between each two electrodes was 1 mm. After connecting to the electrochemical station, we incubated the cell-laden electronic blood vessel for 2 days in DMEM supplemented with 10% FBS (5% CO_2, 37°C). We stained nuclei (blue) with Hoechst 33342 (Invitrogen, USA) and stained the living and dead cells with calcein-AM (green) and PI (red), respectively. We observed the HUVEC proliferation by CLSM (LSM710, Zeiss, Germany) and analyzed the image with ImageJ. We used the CCK-8 kit (Dojindo, Japan) to test the cell viability. We digested cells with 0.25% trypsin (Thermo Fisher, USA) from the substrate and cultured them in a 96-well plate for 6 h. We measured the absorbance at 450 nm using a microplate reader. We analyzed the data using GraphPad Prism 8.

Cell Migration by *In Vitro* Electrical Stimulation

We developed a wound healing model to evaluate cell migration by *in vitro* stimulation. We patterned HUVECs on a PDMS substrate and made a scratch on the cell-laden PDMS substrate using a 10-μL tip. We attached the unfolded electronic blood vessel onto the cell-laden PDMS substrate. We connected the electronic blood vessel to a multichannel electrochemical station (1040C, CHI, China) to generate DC. We used the same parameters as in the proliferation experiment. After 22-h incubation and electrical stimulation, we stained the HUVECs with DiO dye (Life Technologies, USA) and observed HUVEC migration by CLSM (LSM710, Zeiss, Germany) and analyzed the image with ImageJ.

Lyophilization of GFP Plasmid DNA on the MPC-PLC Membrane

We lyophilized the GFP plasmid DNA onto the sterilized MPC-PCL membrane before seeding cells. We added a PDMS chip on top of the MPC-PLC membrane and added 2 mL of the GFP plasmid DNA solution at a concentration of 40 μg mL^{-1} before transferring into a lyophilizer (LGD-0.1, Shanghai Kanxin

Please cite this article in press as: Cheng et al., Electronic Blood Vessel, Matter (2020), https://doi.org/10.1016/j.matt.2020.08.029

Instrument Co., China). The GFP plasmid DNA was dehydrated and fixed on the surface of the MPC-PLC membrane after overnight lyophilization.

In Vitro GFP Plasmid DNA Delivery via Electroporation

We connected the cell-laden MPC-PLC electronic blood vessel with an electroporator (Electro Square Porator ECM 830, BTX, USA). Before electroporation, we washed the samples with PBS solution three times and immersed the cell-laden blood vessel into the GFP plasmid DNA solution (RiboBio, China) at a concentration of 40 μg mL^{-1} for 10 min. We applied five electrical pulses by exerting a square-wave pulse. The voltage was 60 V, the pulse duration 100 μs, and the pulse interval 1 s. After electroporation, we disconnected the electronic blood vessel from the electroporator and incubated it for 2 days in DMEM supplemented with 10% FBS (5% CO_2, 37°C). We respread the electronic blood vessel and fixed the cells with 4% paraformaldehyde aqueous solution for 10 min and performed cytoskeleton staining. After three rinses with fresh PBS, we treated it with 0.1% Triton X-100 solution for 10 min. After three rinses with fresh PBS, we treated it with 3% BSA to avoid non-specific binding activity. We stained the nucleus and F-actin with Hoechst 33342 (Invitrogen, USA) solution (1:1,000 dilution in PBS) for 5 min and then Alexa Fluor 488 phalloidin (Invitrogen, USA) solution (1:200 dilution in PBS) for 20 min. Before imaging, we rinsed the sample five times with PBS solution and mounted it with glycerin solution (70% wt in PBS). We used CLSM (LSM710, Zeiss, Germany) to capture the fluorescence images.

Electroporation on Isolated Rabbit Vascular Tissues

We dissected a 3-cm vascular tissue from the rabbit carotid artery and cut it longitudinally to flatten the tissue. We attached the MPC-PLC membrane lyophilized with the GFP plasmid DNA onto the tissue. After the plasmid DNA dissolved in the fluids, we applied five electrical pulses by exerting a square-wave pulse. The voltage was 60 V, the pulse duration 100 μs, and the pulse interval 1 s. After 2-day incubation in DMEM supplemented with 10% FBS (5% CO_2, 37°C), we stained the nuclei with DAPI and observed the GFP expression by CLSM (LSM710, Zeiss, Germany).

Mechanical Tests of the MPC-PLC Blood Vessel

Stress-Strain Test

We performed the stress-strain test on the MPC-PLC electronic blood vessels, setting the native carotid artery as a control. We used a universal tensile test machine (Instron 3365, USA) to perform the test. We recorded the stress-strain data with Instron Bluehill software. The total length of the tested MPC-PLC electronic blood vessels and native carotid arteries was 30 mm. The gauge length was 15 mm. The drawing speed was set at 10 mm min^{-1} until failure. We processed the data and calculated the ultimate tensile strength, modulus, and strain at break using Origin Pro. Five individual MPC-PLC electronic blood vessels and three individual native carotid arteries were tested.

Burst Pressure and Compliance

We performed the burst pressure and compliance tests using a home-made perfusion system consisting of a pressure gauge (AZ 82100 and AZ 8205, Taiwan) and peristaltic pump (PhdUltra, Harvard Apparatus, USA). We connected the two ends of the MPC-PLC electronic blood vessel or native carotid arteries to two individual PE tubes. We connected the PE tubes with the perfusion system to form a loop. We controlled the pressure inside the loop by adjusting the velocity of flow. We took images of electronic blood vessels with changing diameters

according to the pressure change and recorded the burst pressure. Five individual MPC-PLC electronic blood vessels and three individual native carotid arteries were tested. We used ImageJ (NIH, USA) and Prism (GraphPad, USA) to process the images and measure the diameter changes. We calculated the compliance (C) using the following formulas:

$$D_{inner} = D_{outer} - h_{wall},$$

where D_{inner} and D_{outer} represent the inner and outer diameter of the blood vessels, respectively, and h_{wall} represents the thickness of the wall of the blood vessels, and

$$C = \frac{\frac{D_{inner}(P_2) - D_{inner}(P_1)}{D_{inner}(P_1)}}{P_2 - P_1} \times 10^4,$$

where P_1 and P_2 represent the lower and higher pressure and $D_{inner}(P_1)$ and $D_{inner}(P_2)$ represent the inner diameter during the pressure P_1 and P_2, respectively. The compliance is expressed as percentage diameter change per 100 mm Hg.

In Vivo Study

We conducted the rabbit study in the Center for Cardiovascular Experimental Study and Evaluation in Fuwai Cardiovascular Hospital (FCH, Beijing, China). All the rabbit studies were carried out in compliance with the protocols approved by the Institutional Animal Care and Use Committee at the Center for Cardiovascular Experimental Study and Evaluation of the FCH. Eight rabbits were permitted by the ethics committee to be used as an early stage study. We used New Zealand rabbits (age 200–300 days, body weight 3–4 kg) in this study. We performed an end-to-end anastomosis procedure to implant the MPC-PLC blood vessel on carotid arteries of the rabbits (n = 6). We set two rabbits as a blank control group. We anesthetized the rabbits by injecting 1 mL 3% (3 g 100 mL^{-1}) pentobarbital sodium solution into the auricular vein. The rabbits were connected to an active breathing control system (Primus, Dräger, Germany) and life monitor system (LifeWindow 6000, Digicare, USA), which provided automated anesthesia and ensured active ventilation and *in situ* monitoring. The hair around the neck of the rabbits was removed after sterilization. We incised the epidermal layer to expose the left internal carotid artery. We cross-clamped the proximal and distal ends of the carotid artery with two hemostatic clamps, transected a 1.5-cm segment, and performed end-to-end anastomosis of the electronic blood vessel to the carotid artery (2 cm in length, 2 mm in diameter) by an 8-0 suture (polypropylene, PROLENE blue, Ethicon, USA). After implantation, we tested the blood flow within the MPC-PLC electronic blood vessel using a perivascular flow module (TS410 and TS420, Transonic, USA), which is the gold standard for animal blood flow measurement after implantation. After confirming that the blood flow was strong and smooth, we closed the wound using a 7-0 suture (polypropylene, Surgipro, Covidien, Ireland). After the operation, the rabbits were treated with penicillin (800,000 units per rabbit per day) for 3 days and fed normally. No heparin or any other anticoagulant was used before, during, or after the implantation procedure.

Doppler Ultrasound Imaging

We performed Doppler ultrasound imaging for all the rabbits every 2 weeks for 3 months. We used the Vivid E9 ultrasound system (GE Healthcare, Norway) and a vascular imaging transducer to obtain the 2D and 3D images and videos of the electronic blood vessels. We obtained the color ultrasonography, synchronized pulse of the operative site, and corresponding blood flow velocity. We measured the diameter of the electronic blood vessels from different directions. All the results were saved as pictures and videos.

Please cite this article in press as: Cheng et al., Electronic Blood Vessel, Matter (2020), https://doi.org/10.1016/j.matt.2020.08.029

Arteriography

We performed arteriography for all the rabbits every month for 3 months. We anesthetized the rabbits by injecting 1 mL 3% (3 g 100 mL^{-1}) pentobarbital sodium solution into the auricular vein. The rabbits were connected to the active breathing control system (Primus, Dräger, Germany) and life monitor system (LifeWindow 6000, Digicare, USA), which provided automated anesthesia and ensured the active ventilation and *in situ* monitoring. We used a cardiovascular and interventional imaging system (Innova 2100-IQ, GE Medical Systems SCS, GE Healthcare, France) to diagnose the patency of the MPC-PLC electronic blood vessels. Iopromide contrast medium (Ultravist 370) was injected into the vascular system to visualize the blood vessel and blood flow in real time via digital subtraction angiography. The electronic blood vessel exhibited autoradiography under the arteriography due to the existence of LMP-based circuits. All the diagnosis results were saved as pictures and videos.

Blood Test

Following the ultrasound imaging at each time point, we extracted a 3-mL blood sample from the rabbits for inflammation and infection tests, including routine blood examination, biochemical tests, and ELISA of three important proteins, i.e., IL-6, PCT, and CRP. Two milliliters of blood was sent to the Fuwai hospital for the routine blood examination and biochemical tests. One milliliter of blood was processed in the lab for ELISA. We collected all the samples and tested them at the end time point using three rabbit ELISA kits (Rabbit IL-6 ELISA kit, PCT ELISA kit, and CRP ELISA kit, MyBioSource, USA).

Ex Vivo Study

We explanted all the MPC-PLC electronic blood vessels and the major organs, including heart, liver, spleen, lung, and kidney, 3 months post-implantation. In the meantime, we also sacrificed two normal rabbits in the blank control group to obtain the native carotid artery and their major organs. We preserved all the samples in 4% paraformaldehyde aqueous solution separately. Part of the samples was dehydrated using an automatic tissue dehydrating machine (ASP200s, Leica, Germany) and paraffin-embedded using a paraffin-embedding machine (EG1150 System, Leica, Germany). We cut the samples into 6-μm-thick sections using a microtome (RM2235, Leica, Germany) and de-paraffinized the samples twice (10 min each time) with dimethylbenzene and serially rinsed with 100% ethanol, 90% ethanol, 80% ethanol, 70% ethanol, and deionized water for 5 min each step. We stained the cross sections of the MPC-PLC electronic blood vessels and the native carotid arteries with H&E, Masson's trichrome, and Verhoeff's and affixed the stained sections to coverslips with Gelvatol mounting medium. We stained the cross sections of the major organs from the MPC-PLC electronic blood vessel-implanted group and the control group with H&E and Masson's trichrome and affixed the stained sections to coverslips with Gelvatol mounting medium. We captured the images using an upright microscope (DM4000M, Leica, Germany). All the images are representative of at least three independent samples.

Statistical Analysis

We conducted image analysis of LMPs, MPC-PLC membrane, mechanical test data, and Doppler ultrasound data using ImageJ (NIH, USA) and Prism 8 (GraphPad, USA). We recorded the stress-strain data using Instron Bluehill software (Instron, USA). All the statistical data are expressed as the mean ± SD with a group number n described in the figure caption.

SUPPLEMENTAL INFORMATION

Supplemental Information can be found online at https://doi.org/10.1016/j.matt.2020.08.029.

ACKNOWLEDGMENTS

This study was supported by the National Key R&D Program of China (2018YFA0902600, 2017YFA0205901), the National Natural Science Foundation of China (21535001, 81730051, 21761142006, 51973045), the Chinese Academy of Sciences (QYZDJ-SSW-SLH039, 121D11KYSB20170026, XDA16020902), Shenzhen Bay Laboratory (SZBL2019062801004), the Tencent Foundation through the XPLORER prize, the Beijing Science and Technology Plan Project (Z191100007619053), the Postgraduate Innovation Foundation of Peking Union Medical College (2019-1002-28), and the Teaching Reform Foundation of Postgraduate Education in Peking Union Medical College (10023201900202). We thank Dr. Zewen Wei and Dr. Deyao Zhao for discussions on the electroporation experiment. We thank Mrs. Barbara Althaus at EPFL for her advice in writing the manuscript.

AUTHOR CONTRIBUTIONS

X.J. and S.C. conceived the idea. S.C. designed the experiments; fabricated the blood vessel; conducted the characterization, *in vitro* tests, mechanical tests, *in vivo* tests, and *ex vivo* tests; analyzed the data; and wrote the manuscript. C.H. fabricated the blood vessel and performed *in vitro* tests, mechanical tests, and *in vivo* tests. L.D. performed *in vivo* and *ex vivo* tests. S.C., C.H., and L.D. contributed equally. L.T. assisted with the preparation of the liquid metal particles and the MPC-PLC membrane and the electroporation experiments. L.J. and Y.Z. performed the implantation of the electronic blood vessel, Doppler ultrasound imaging, and arteriography. L.M. conducted the ELISA. J.Q. and R.D. assisted in the transmission electron microscopy characterization. W.Z. gave input on the *in vitro* tests and *ex vivo* tests. Y.Z. supervised the *in vivo* and *ex vivo* study. X.J. supervised the project and revised the manuscript. All the authors took part in the discussion and writing.

DECLARATION OF INTERESTS

S.C. and X.J. declare financial interest in the form of a patent application. Other authors declare no competing financial interests.

Received: May 7, 2020
Revised: August 11, 2020
Accepted: August 26, 2020
Published: October 1, 2020

REFERENCES

1. WHO (2019). World Health Statistics 2019: Monitoring Health for the SDGs (World Heal. Organ.).

2. Seifu, D.G., Purnama, A., Mequanint, K., and Mantovani, D. (2013). Small-diameter vascular tissue engineering. Nat. Rev. Cardiol. *10*, 410–421.

3. Quint, C., Kondo, Y., Manson, R.J., Lawson, J.H., Dardik, A., and Niklason, L.E. (2011). Decellularized tissue-engineered blood vessel as an arterial conduit. Proc. Natl. Acad. Sci. U S A *108*, 9214–9219.

4. Dahl, S.L., Kypson, A.P., Lawson, J.H., Blum, J.L., Strader, J.T., Li, Y., Manson, R.J., Tente, W.E., DiBernardo, L., Hensley, M.T., et al. (2011). Readily available tissue-engineered vascular grafts. Sci. Transl. Med. *3*, 68ra9.

5. Lawson, J.H., Glickman, M.H., Ilzecki, M., Jakimowicz, T., Jaroszynski, A., Peden, E.K., Pilgrim, A.J., Prichard, H.L., Guziewicz, M., Przywara, S., et al. (2016). Bioengineered human acellular vessels for dialysis access in patients with end-stage renal disease: two phase 2 single-arm trials. Lancet *387*, 2026–2034.

6. Zhu, M., Li, W., Dong, X., Yuan, X., Midgley, A.C., Chang, H., Wang, Y., Wang, H., Wang, K., Ma, P.X., et al. (2019). In vivo engineered extracellular matrix scaffolds with instructive niches for oriented tissue regeneration. Nat. Commun. *10*, 4620.

7. Kirkton, R.D., Santiago-Maysonet, M., Lawson, J.H., Tente, W.E., Dahl, S.L.M., Niklason, L.E., and Prichard, H.L. (2019). Bioengineered human acellular vessels recellularize and evolve into living blood vessels after human implantation. Sci. Transl. Med. *11*, 1–12.

8. L'Heureux, N., Dusserre, N., Konig, G., Victor, B., Keire, P., Wight, T.N., Chronos, N.A., Kyles, A.E., Gregory, C.R., Hoyt, G., et al. (2006). Human tissue-engineered blood vessels for adult arterial revascularization. Nat. Med. *12*, 361–365.

9. L'Heureux, N., McAllister, T.N., and de la Fuente, L.M. (2007). Tissue-engineered blood vessel for adult arterial revascularization. N. Engl. J. Med. *357*, 1451–1453.

10. L'Heureux, N., Dusserre, N., Marini, A., Garrido, S., de la Fuente, L., and McAllister, T. (2007). Technology insight: the evolution of tissue-engineered vascular grafts - from research to clinical practice. Nat. Clin. Pract. Cardiovasc. Med. *4*, 389–395.

11. Peck, M., Dusserre, N., McAllister, T.N., and L'Heureux, N. (2011). Tissue engineering by self-assembly. Mater. Today *14*, 218–224.

12. Wu, W., Allen, R.A., and Wang, Y. (2012). Fast-degrading elastomer enables rapid remodeling of a cell-free synthetic graft into a neoartery. Nat. Med. *18*, 1148–1153.

13. Cheng, S., Jin, Y., Wang, N., Cao, F., Zhang, W., Bai, W., Zheng, W., and Jiang, X. (2017). Self-Adjusting, polymeric multilayered roll that can keep the shapes of the blood vessel scaffolds during biodegradation. Adv. Mater. *29*, 1700171.

14. Akentjew, T.L., Terraza, C., Suazo, C., Maksimcuka, J., Wilkens, C.A., Vargas, F., Zavala, G., Ocaña, M., Enrione, J., García-Herrera, C.M., et al. (2019). Rapid fabrication of reinforced and cell-laden vascular grafts structurally inspired by human coronary arteries. Nat. Commun. *10*, 1–15.

15. Hoenig, M.R., Campbell, G.R., Rolfe, B.E., and Campbell, J.H. (2005). Tissue-engineered blood vessels: alternative to autologous grafts? Arterioscler. Thromb. Vasc. Biol. *25*, 1128–1134.

16. Yan, J., Lu, Y., Chen, G., Yang, M., and Gu, Z. (2018). Advances in liquid metals for biomedical applications. Chem. Soc. Rev. *47*, 2518–2533.

17. Choi, S., Han, S.I., Kim, D., Hyeon, T., and Kim, D.H. (2019). High-performance stretchable conductive nanocomposites: materials, processes, and device applications. Chem. Soc. Rev. *48*, 1566–1595.

18. Son, D., Lee, J., Lee, D.J., Ghaffari, R., Yun, S., Kim, S.J., Lee, J.E., Cho, H.R., Yoon, S., Yang, S., et al. (2015). Bioresorbable electronic stent integrated with therapeutic nanoparticles for endovascular diseases. ACS Nano *9*, 5937–5946.

19. Du, Z.J., Bi, G.Q., and Cui, X.T. (2018). Electrically controlled neurochemical release from dual-layer conducting polymer films for precise modulation of neural network activity in rat barrel cortex. Adv. Funct. Mater. *28*, 1–12.

20. Gong, P., et al. (2013). A strategy for the construction of controlled, three-dimensional, multilayered, tissue-like structures. Adv. Funct. Mater. *23*, 42–46.

21. Jin, Y., Wang, N., Yuan, B., Sun, J., Li, M., Zheng, W., Zhang, W., and Jiang, X. (2013). Stress-induced self-assembly of complex three dimensional structures by elastic membranes. Small *9*, 2410–2414.

22. Yuan, B., Jin, Y., Sun, Y., Wang, D., Sun, J., Wang, Z., Zhang, W., and Jiang, X. (2012). A strategy for depositing different types of cells in three dimensions to mimic tubular structures in tissues. Adv. Mater. *24*, 890–896.

23. Wang, N., Tang, L., Zheng, W., Peng, Y., Cheng, S., Lei, Y., Zhang, L., Hu, B., Liu, S., Zhang, W., et al. (2016). A strategy for rapid and facile fabrication of controlled, layered blood vessel-like structures. RSC Adv. *6*, 55054–55063.

24. Tang, L., Mou, L., Zhang, W., and Jiang, X. (2019). Large-scale fabrication of highly elastic conductors on a broad range of surfaces. ACS Appl. Mater. Inter. *11*, 7138–7147.

25. Tang, L., Cheng, S., Zhang, L., Mi, H., Mou, L., Yang, S., Huang, Z., Shi, X., and Jiang, X. (2018). Printable metal-polymer conductors for highly stretchable bio-devices. iScience *4*, 302–311.

26. Bai, H., McCaig, C.D., Forrester, J.V., and Zhao, M. (2004). DC electric fields induce distinct preangiogenic responses in microvascular and macrovascular cells. Arterioscler. Thromb. Vasc. Biol. *24*, 1234–1239.

27. Lu, Y., Hu, Q., Lin, Y., Pacardo, D.B., Wang, C., Sun, W., Ligler, F.S., Dickey, M.D., and Gu, Z. (2015). Transformable liquid-metal nanomedicine. Nat. Commun. *6*, 10066.

28. Kenar, H., Ozdogan, C.Y., Dumlu, C., Doger, E., Kose, G.T., and Hasirci, V. (2019). Microfibrous scaffolds from poly(L-lactide-co-ϵ-caprolactone) blended with xeno-free collagen/hyaluronic acid for improvement of vascularization in tissue engineering applications. Mater. Sci. Eng. C *97*, 31–44.